Contemporary Mathematics

Reduced-order Modeling of Navier-Stokes equations via Cenroidal Voronoi Tessellation

Max Gunzburger and Hyung-Chun Lee

Abstract. A reduced-basis method based on centroidal Voronoi tessellations (CVT's) is introduced. A discussion of reduced-ordering modeling for complex systems such as fluid flows is given to provide a context for the application of reduced-order bases. Then, detailed descriptions of CVT-based reduced-order bases including their construction from snapshot sets and their application to the low-cost simulation of complex systems are given. Some concrete incompressible flow examples are used to illustrate the construction and use of CVT-based reduced-order bases.

1. Introducion

Numerical solutions of nonlinear complex systems such as the Navier-Stokes system are expensive with respective to both storage and CPU costs. Even with the use of good mesh generators, discretization schemes, and solution algorithms, the computational simulation of complex, turbulent, or chaotic systems still remains a formidable endeavor. For example, typical finite element codes may require many thousands of degrees of freedom for the accurate simulation of fluid flows. The situation is even worse for optimization problems for which multiple solutions of the complex state system are usually required or in feedback control problems for which real-time solutions of the complex state system are needed. The types of reduced-order models that we study are those that attempt to determine accurate approximate solutions of a complex system using very few degrees of freedom. To do so, such models have to use basis functions that are in some way intimately connected to the problem being approximated. Once a very low-dimensional reduced basis has been determined, one can employ it to solve the complex system by applying, e.g., a Galerkin method. There have been many reduced-order modeling techniques proposed. The most popular reduced-order modeling approach for complex systems is based on proper orthogonal decomposition (POD) analysis. POD begins with a set of $\widetilde{m}$ snapshots; these could be generated by evaluating the computational solution of a transient problem at several instants of time or by evaluating the computational solution for several values of the parameters appearing in the problem description or by a combination of the two. The computational solutions that are used to determine the snapshot set are determined using costly,

This work was supported by KOSEF R01-2000-000-00008-0.

large-scale, high-fidelity, e.g., finite element, codes. The K-dimensional POD basis is then determined from the K eigenvectors corresponding to the $\widetilde{d}$ most dominant eigenvalues of the correlation matrix for the snapshots. The POD basis is then used, usually by applying a projection procedure, to determine an approximate solution for different values of the system parameters. POD-based model reduction has been applied with some success to several problems, most notably in fluid mechanics settings. For detailed discussions, one may consult [1–8, 10–27].

Centroidal Voronoi tessellations (CVT's) have been successfully used in several data compression settings, e.g., in image processing and the clustering of data. Reduced-order modeling of complex systems is another data compression setting, i.e., replacing high-dimensional approximations with low-dimensional ones. Thus, one can ask if CVT's can be used for the reduced-order modeling of complex systems? In CVT-reduced order modeling, we start with a snapshot set just as is done in a POD-based setting. However, instead of determining a POD basis from the snapshot set, we apply our CVT methodologies to determine the generators of a CVT of the snapshot set; these generators constitute the reduced-order basis. We then use the CVT-based basis in just the same way as one uses a POD-based basis to determine a very low-dimensional approximation to the solution of a complex system. CVT also possesses an optimality property, although it is different from that possessed by POD bases.

The efficiency of CVT-based reduced bases depends on the their dimension, i.e., if a CVT-based basis is low-dimensional and can still approximate the state well, then approximations of the state of a complex system can be inexpensively determined. However, the ability of a CVT-based basis to approximate the state of a system is totally dependent on the information contained in the snapshot set used to generate the basis. Certainly, a CVT-based basis cannot contain more information than that contained in the snapshot set. Thus, crucial to the success of the CVT-based approaches to model reduction is the generation of "good" snapshot sets. (All this is equally true for POD-based bases.)

2. The CVT reduced-basis method for the Navier-Stokes equations

Let Ω be a bounded region in $\Re^2$ whose boundary is denoted by $\partial\Omega = \Gamma_D \cup \Gamma_N$ and let T denote a positive constant. Let $\mathbf{u}(t, \mathbf{x})$ and $p(t, \mathbf{x})$ denote the velocity and pressure fields, respectively, $\mathbf{f}(t, \mathbf{x})$ the given body force per unit mass, and $\mathbf{u}_0$ the given initial velocity. Furthermore, let $\mathbf{b}$ denote a specified the boundary velocity. The Navier-Stokes equations are then given by

$$\mathbf{u}_t - \nu\Delta\mathbf{u} + (\mathbf{u}\cdot\nabla)\mathbf{u} + \nabla p = \mathbf{f} \quad \text{in } \Omega \times (0, T] \tag{2.1}$$

$$\nabla\cdot\mathbf{u} = 0 \quad \text{in } \Omega \times (0, T] \tag{2.2}$$

$$\mathbf{u} = \mathbf{b} \quad \text{on } \Gamma_D \times (0, T] \tag{2.3}$$

$$-p + \nu\frac{\partial\mathbf{u}}{\partial n} = \mathbf{0} \quad \text{on } \Gamma_N \times (0, T] \tag{2.4}$$

$$\mathbf{u}(0, \mathbf{x}) = \mathbf{u}_0(\mathbf{x}) \quad \text{in } \Omega, \tag{2.5}$$

where ν is the kinetic viscosity.

2.1. Variational formulation. We use a variational formulation and finite element method to approximate (2.1)–(2.5), but other methods can be also used in the context of reduced-basis methods.

A variational formulation of the problem (2.1)–(2.5) is following: Find $\mathbf{u} \in L^2(0,T;\mathbf{V}_b)$ and $p \in L^2(0,T;L_0^2(\Omega))$ such that

$$\int_\Omega \mathbf{u}_t \cdot \mathbf{v}\, d\Omega + \nu \int_\Omega \nabla\mathbf{u} : \nabla\mathbf{v}\, d\Omega + \int_\Omega (\mathbf{u}\cdot\nabla)\mathbf{u}\cdot\mathbf{v}\, d\Omega - \int_\Omega p\nabla\cdot\mathbf{v}\, d\Omega$$
$$= \int_\Omega \mathbf{f}\cdot\mathbf{v}\, d\Omega \quad \text{for all } \mathbf{v} \in \mathbf{H}_0^1(\Omega) \tag{2.6}$$

$$\int_\Omega q\nabla\cdot\mathbf{u} d\Omega = 0 \quad \text{for all } q \in L_0^2(\Omega) \tag{2.7}$$

$$\mathbf{u}(0,\mathbf{x}) = \mathbf{u}_0(\mathbf{x}) \quad \text{in } \Omega, \tag{2.8}$$

where $\mathbf{V}_b = \{\mathbf{u} \in \mathbf{H}^1(\Omega) \,:\, \mathbf{u} = \mathbf{b} \text{ on } \Gamma_D, \mathbf{b} \in \mathbf{H}^{1/2}(\partial\Omega)\}$ and $\mathbf{H}_0^1 = \{\mathbf{u} \in \mathbf{H}^1(\Omega) \,:\, \mathbf{u} = \mathbf{0} \text{ on } \Gamma_D\}$.

A typical finite element approximation of (2.6)–(2.7) is to seek solutions $\mathbf{u}^h(t,\cdot) \in \mathbf{V}_b^h \subset \mathbf{V}_b$ and $p^h \in S_0^h \subset L_0^2(\Omega)$,

$$\int_\Omega \mathbf{u}_t^h \cdot \mathbf{v}^h\, d\Omega + \nu \int_\Omega \nabla\mathbf{u}^h : \nabla\mathbf{v}^h\, d\Omega + \int_\Omega (\mathbf{u}^h\cdot\nabla)\mathbf{u}^h\cdot\mathbf{v}^h\, d\Omega$$
$$- \int_\Omega p^h\nabla\cdot\mathbf{v}^h\, d\Omega = \int_\Omega \mathbf{f}\cdot\mathbf{v}^h\, d\Omega \quad \text{for all } \mathbf{v}^h \in \mathbf{V}_0^h \tag{2.9}$$

$$\int_\Omega q^h\nabla\cdot\mathbf{u}^h d\Omega = 0 \quad \text{for all } q^h \in S_0^h \tag{2.10}$$

where $\mathbf{V}_0^h \subset \mathbf{H}_0^1(\Omega)$ and $S_0^h \subset L_0^2(\Omega)$.

2.2. Centroidal Voronoi tessellations. Given a discrete set of modified snapshots $W = \{\vec{u}_n\}_{n=1}^N$ (see Section 3.1 for a discussion of snapshots, including how they are generated and how they are modified to satisfy zero boundary conditions) belonging to $\Re^J$, a set $\{V_k\}_{k=1}^K$ is a tessellation of W if $\{V_k\}_{k=1}^K$ is a subdivision of W into disjoint, covering subsets, i.e., $V_k \subset W$ for $k = 1, ..., K$, $V_k \cap V_i = \emptyset$ for $k \neq i$, and $\bigcup_{k=1}^K V_k = W$. Given a set of points $\{\vec{z}_k\}_{k=1}^K$ belonging to $\Re^J$ (but not necessarily to W), the *Voronoi region* corresponding to the point $\vec{z}_k$ is defined by

$$\widehat{V}_k = \{\vec{u} \in W \;:\; |\vec{u} - \vec{z}_k| \leq |\vec{u} - \vec{z}_i| \quad \text{for} \quad i = 1, ..., K,\ k \neq i\},$$

where equality holds only for $k < i$. The set $\{\widehat{V}_k\}_{k=1}^K$ is called *Voronoi tessellation* or *Voronoi diagram* of W corresponding to the set of points $\{\vec{z}_k\}_{k=1}^K$. The points $\vec{z}_k$, $k = 1, \ldots, K$, are called the generators of the Voronoi diagram $\{\widehat{V}_k\}_{k=1}^K$ of W. Given a density function $\rho(\vec{y}) \geq 0$, defined for $\vec{y} \in W$, the *mass centroid* $\vec{z}^*$ of any subset $V \subset W$ is defined by

$$\sum_{\vec{y}\in V} \rho(\vec{y})|\vec{y} - \vec{z}^*|^2 = \inf_{\vec{z}\in V^*} \sum_{\vec{y}\in V} \rho(\vec{y})|\vec{y} - \vec{z}|^2,$$

where the sums extend over the points belonging to V. The set V^* can be taken to be V or it can be an even larger set such as all of $\Re^J$. In case $V^* = \Re^J$, $\vec{z}^*$ is the ordinary mean

$$\vec{z}^* = \frac{\sum_{\vec{y}\in V} \rho(\vec{y})\vec{y}}{\sum_{\vec{y}\in V} \rho(\vec{y})}.$$

In this case, $\vec{z}^* \notin W$ in general.

If $\{\vec{z}_k\}_{k=1}^K$ is the set of generating points of the Voronoi tessellation $\{\widehat{V}_k^K\}$ and $\{\vec{z}_k^*\}_{k=1}^K$ is the set of mass centroids of the Voronoi regions $\{\widehat{V}_k^K\}$, then, in general,

$\vec{z}_k \neq \vec{z}_k^*$ for $k = 1, ..., K$. If $\vec{z}_k = \vec{z}_k^*$ for $k = 1, ..., K$, then we refer to the Voronoi tessellation as being a *centroidal Voronoi tessellation* (CVT). CVT's of discrete sets are closely related to optimal K-means clusters so that Voronoi regions and centroids can be referred to as clusters and cluster centers, respectively.

There are several algorithms known for constructing centroidal Voronoi tessellations of a given set. Lloyd's method is a deterministic algorithm which is the obvious iteration between computing Voronoi diagrams and mass centroids, i.e., a given set of generators is replaced in an iterative process by the mass centroids of the Voronoi regions corresponding to those generators. MacQueen's method is a very elegant probabilistic algorithm. Other probabilistic methods have been devised that may be viewed as generalization of both the MacQueen and Lloyd methods and that are amenable to efficient parallelization; see [9].

2.3. The CVT reduced-order model. If $\{\vec{z}_k\}_{k=1}^K$ are the generators of a CVT of the set of (modified) snapshot vectors $\{\vec{u}_n\}_{n=1}^N$, we choose for the reduced-basis space

$$\mathbf{U}^K = \text{span}\{\mathbf{z}_k \,:\, i = k, \ldots, K\},$$

where, for $k = 1, \ldots, K$, $\mathbf{z}_k$ is the finite element function having $\vec{z}_k$ as coefficients. As will be illustrated in Section 3.1, the reduced-basis functions satisfy homogeneous boundary conditions. We then seek a reduced-basis approximation of the form $\mathbf{u}^K(t,\cdot) = \mathbf{u}_p^K(t,\cdot) + \mathbf{u}_h^K(t,\cdot)$, where $\mathbf{u}_h^K(t,\cdot) \in \mathbf{U}^K = \text{span}\{\mathbf{u}_k \,:\, k = 1, \ldots, K\} \subset \mathbf{V}^h$ and $\mathbf{u}_p^K(t,\cdot)$ is a particular finite element function chosen to satisfy the boundary conditions (again, see Section 3.1); $\mathbf{u}_h^K(t,\cdot)$ is determined from

$$\int_\Omega \mathbf{u}_t^K \cdot \mathbf{v}\, d\Omega + \nu \int_\Omega \nabla \mathbf{u}^K : \nabla \mathbf{v}\, d\Omega + \int_\Omega (\mathbf{u}^K \cdot \nabla)\mathbf{u}^K \cdot \mathbf{v}\, d\Omega = \int_\Omega \mathbf{f} \cdot \mathbf{v}\, d\Omega \quad \forall \mathbf{v} \in \mathbf{U}^K \tag{2.11}$$

$$(\mathbf{u}^K, \mathbf{v})_{\partial\Omega} = (\mathbf{u}_b, \mathbf{v})_{\partial\Omega} \quad \forall \mathbf{v} \in \mathbf{U}^K|_{\partial\Omega}, \tag{2.12}$$

and

$$(\mathbf{u}(0,\mathbf{x}), \mathbf{v}^M) = (\mathbf{u}_0(\mathbf{x}), \mathbf{v}) \quad \text{for all } \mathbf{v} \in \mathbf{U}^K. \tag{2.13}$$

Note that the pressure does not appear in these equations; also, the continuity equation (2.2) is absent. This is because the reduced basis functions are constructed so that they are automatically discretely divergence free.

In our computational example, because of the special form chosen for the inhomogenous data $\mathbf{b}$, we will be able to choose the particular solution $\mathbf{u}_p^K(t,\mathbf{x})$ to have the form $\mathbf{u}_p^K = \alpha_0(t)\boldsymbol{\phi}_0(\mathbf{x})$, where $\boldsymbol{\phi}_0$ is a steady-state finite element solution of the discretized Navier-Stokes equations and $\alpha_0(t)$ is chosen so that $\mathbf{u}_p^K(t,\mathbf{x})$ satisfies the time-dependent boundary condition. If we let $\boldsymbol{\phi}_k = \mathbf{u}_k$ for $k = 1, \ldots, K$, then the reduced-basis approximation of the velocity takes the form

$$\mathbf{u}^K(t) = \sum_{k=0}^K \alpha_k(t)\phi_k. \tag{2.14}$$

Then, (2.11) and (2.13) respectively take the form

$$\sum_{k=0}^{K} \frac{d}{dt}\alpha_k(t)(\boldsymbol{\phi}_k,\boldsymbol{\phi}_k) + \nu \sum_{k=0}^{K} \alpha_k(t)(\nabla\boldsymbol{\phi}_k,\nabla\boldsymbol{\phi}_i) + \left(\sum_{\ell=0}^{K} \alpha_\ell(t)\boldsymbol{\phi}_\ell \cdot \nabla \sum_{i=0}^{k} \alpha_k(t)\boldsymbol{\phi}_k, \boldsymbol{\phi}_i\right) = (\mathbf{f},\boldsymbol{\phi}_i) \tag{2.15}$$

and

$$\sum_{i=1}^{k} \alpha_k(0)(\boldsymbol{\phi}_k,\boldsymbol{\phi}_i) = (\mathbf{u}_0,\boldsymbol{\phi}_i) \tag{2.16}$$

for $i = 1,\ldots,K$. Equivalently, we have the nonlinear system of ordinary differential equations that determine $\{\alpha_k(t)\}_{k=1}^{K}$

$$\mathbb{M}\frac{d}{dt}\vec{\alpha}(t) + \mathbb{H}\vec{\alpha}(t) + (\vec{\alpha}(t))^T\mathbb{N}\vec{\alpha}(t) = \vec{f}(t) \tag{2.17}$$

where the mass matrix $\mathbb{M}$, the stiffness matrix $\mathbb{H}$, the solution vector $\vec{\alpha}(t)$, the convection tensor $\mathbb{N}$, and the forcing vector $\vec{f}(t)$ are respectively given by

$$\mathbb{M}_{ik} = \int_\Omega \boldsymbol{\phi}_k \cdot \boldsymbol{\phi}_i \, d\Omega, \qquad \mathbb{H}_{ik} = \nu \int_\Omega \nabla\boldsymbol{\phi}_k : \nabla\boldsymbol{\phi}_i \, d\Omega, \qquad (\vec{\alpha})_k = \alpha_k(t),$$
$$\mathbb{N}_{i\ell k} = \int_\Omega (\boldsymbol{\phi}_\ell \cdot \nabla)\boldsymbol{\phi}_k \cdot \boldsymbol{\phi}_i \, d\Omega, \qquad (\vec{f})_i = \int_\Omega \mathbf{f} \cdot \boldsymbol{\phi}_i \, d\Omega$$

for $k,i,\ell = 1,\ldots,K$. Note that some terms on the left-hand side of (2.17) involve α_0 only (and not the other α_k's); those terms should be shifted to the right-hand side. Also note that all of these matrices and tensors are full; however, since K will be chosen small (see Section 3.2), this does not cause any computational inefficiencies.

3. Computational experiments illustrating the mplementation of the CVT-reduced-order model

To compare the use, efficiency, and accuracy of the CVT-based reduced-order modeling technique, one example is considered, which we denote the *T-Cell problem.* This is a incompressible, viscous flow problem having boundary conditions that include an inflow shape function containing a multiplicative parameter γ that controls the strength of the inflow.

The governing equations for the two dimensional incompressible, viscous flow in the T-shaped region (see Figure 1) are the Navier-Stokes system (2.1) and (2.2) (with $\mathbf{f} = \mathbf{0}$) along with, for the specific problems considered here, the initial and boundary conditions

$$\mathbf{u}(0,\mathbf{x}) = \mathbf{u}_0(\mathbf{x}) \qquad \text{in} \quad \Omega, \tag{3.1}$$
$$\mathbf{u} = 100\,\gamma(t)\,(1-y)\,(0.5-y) \qquad \text{on} \quad (0,T)\times\Gamma_i, \tag{3.2}$$
$$-p + (\mathbf{n}\cdot\nabla)\,\mathbf{u} = 0 \qquad \text{on} \quad (0,T)\times\Gamma_o, \tag{3.3}$$
$$\mathbf{u} = 0 \qquad \text{on} \quad (0,T)\times\Gamma_d, \tag{3.4}$$

where $\mathbf{x} = (x,y)$, $\Gamma_i = \{x = 0\,;\, 0.5 < y < 1.0\}$ and $\Gamma_o = \{x = 1\,;\, 0.5 < y < 1.0\}$ are the inflow and outflow parts of the boundary, respectively, and $\Gamma_d = \partial\Omega\backslash(\overline{\Gamma}_i \cup \overline{\Gamma}_o)$; see Figure 1. In (3.2), $\gamma(t)$ is a parameter that determines the strength of the

parabolic inflow velocity profile. We choose $\nu = 1$ and $T = 0.05$ for generating snapshots.

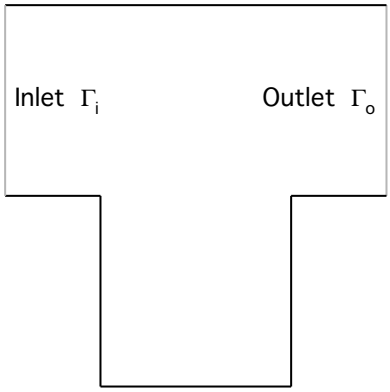

FIGURE 1. The flow region for the T-Cell example.

Accurate Galerkin-mixed method finite element approximations of the solutions of (2.1), (2.2), and (3.1)–(3.4) are obtained using the $P2$–$P1$ Taylor-Hood finite element pair on a grid of 4961 nodes. Finite element solutions are used for the generation of snapshots and later for comparison with CVT-based reduced-order solutions.

For the generation of snapshots, we will also solve, by the finite element method, stationary versions of our governing system for which the time derivative term in (2.1) and the initial condition (3.1) are omitted and γ in (3.2) is chosen independent of t.

3.1. Generating snapshots. We use the following procedure to determine a set of snapshot vectors. First, the finite element approximation to the stationary version of (2.1), (2.2), and (3.1)–(3.4) with $\gamma = 1$ is obtained. Using that steady state solution as the initial data $\mathbf{u}_0$ in (3.1) and using $\gamma = 5$ for $0 < t < T/2 = 0.025$ and $\gamma = 1$ for $0.025 < t < T = 0.05$ in the boundary condition (3.2), we then determine a finite element approximation $\sum_{j=1}^{J} U_j(t)\boldsymbol{\psi}_j(\mathbf{x})$ of the solution of (2.1), (2.2), and (3.1)–(3.4), where J denotes the dimension of the finite element space used for the velocity and $\{\boldsymbol{\psi}_j\}_{j=1}^{J}$ denotes the basis functions for that space. This is the flow we use to generate the snapshots; it can be viewed as one for which the steady state solution for $\gamma = 1$ is suddenly jolted, at $t = 0$, by increasing the value of γ to five, and jolted again at $t = T/2 = 0.025$ by decreasing the value of γ back to one. The 500 snapshot vectors

$$\vec{u}_n = \begin{pmatrix} U_1(t_n) \\ U_2(t_n) \\ \vdots \\ U_J(t_n) \end{pmatrix}, \quad n = 1, \ldots, N = 500, \tag{3.5}$$

are then determined by evaluating the solution of this impulsively started problem at 500 equally spaced time values t_n, $n = 1, \ldots, 500$, ranging from $t = 0$ to $t = T = 0.05$. Note that the time interval used for sampling snapshots is a multiple

of the time interval used for the time discretization of the system of ordinary differential equations (2.17). The snapshot vectors $\{\vec{u}_n\}_{n=1}^N$ correspond to the snapshot functions

$$\mathbf{u}_n(\mathbf{x}) = \sum_{j=1}^{J} U_j(t_n)\boldsymbol{\psi}_j(\mathbf{x}) \qquad \text{for } n = 1, \ldots, N = 500.$$

For subsequent use, it is convenient to modify the 500 snapshots so that they satisfy homogeneous boundary conditions. To this end, we first obtain the reference finite element approximation $\mathbf{v}(\mathbf{x}) = \sum_{j=1}^{J} V_j\boldsymbol{\psi}_j(\mathbf{x})$ of the stationary version of (2.1), (2.2), and (3.1)–(3.4) with $\gamma = 3$. We then modify the first 250 snapshots by

$$\mathbf{u}_n \leftarrow \left(\mathbf{u}_n - \frac{5}{3}\mathbf{v}\right) \qquad \text{or} \qquad \vec{u}_n \leftarrow \left(\vec{u}_n - \frac{5}{3}\vec{v}\right) \quad \text{for } n = 1, \ldots, 250.$$

and, in the same way, the second 250 snapshots are modified

$$\mathbf{u}_n \leftarrow \left(\mathbf{u}_n - \frac{1}{3}\mathbf{v}\right) \qquad \text{or} \qquad \vec{u}_n \leftarrow \left(\vec{u}_n - \frac{1}{3}\vec{v}\right) \quad \text{for } n = 251, \ldots, 500,$$

where

$$\vec{v} = \begin{pmatrix} V_1 \\ V_2 \\ \vdots \\ V_J \end{pmatrix}.$$

In this way, all the snapshots satisfy homogeneous boundary conditions.

3.2. Generating the CVT reduced basis. For a given K, we next apply a CVT-generation algorithm to the snapshot set; the resulting set of CVT generators is to be used as a reduced basis. CVT's of the snapshot set having $K = 4$, 5, 6, 7, 8, 10, 12 and 16 generators are determined in this manner. Figure 2 displays, for the $K = 8$ generator case, the CVT basis computed from the modified snapshots. Note that since the original boundary conditions have been "subtracted away," each basis function satisfies a zero Dirichlet boundary condition at the inlet, and a zero Neumann condition at the outlet. In the interior of the region, each basis function satisfies the (discretized) continuity equation. It is important to note that the CVT-basis set of size 8 is not built by augmenting a CVT-basis of smaller cardinality; in general, one observes that elements of two CVT-bases generated from the same snapshot set but having different cardinalities seem to differ significantly.

Each generator $\vec{z}_k \in \Re^K$ of a CVT defines a finite element function, i.e., if

$$\vec{z}_k = \begin{pmatrix} Z_1^k \\ Z_2^k \\ \vdots \\ Z_J^k \end{pmatrix} \quad \text{for } k = 1, \ldots, K$$

denote the CVT basis vectors, we then have the corresponding finite element functions

$$\mathbf{z}_k = \sum_{j=1}^{J} Z_j^k\boldsymbol{\psi}_j(\mathbf{x}) \quad \text{for } k = 1, \ldots, K.$$

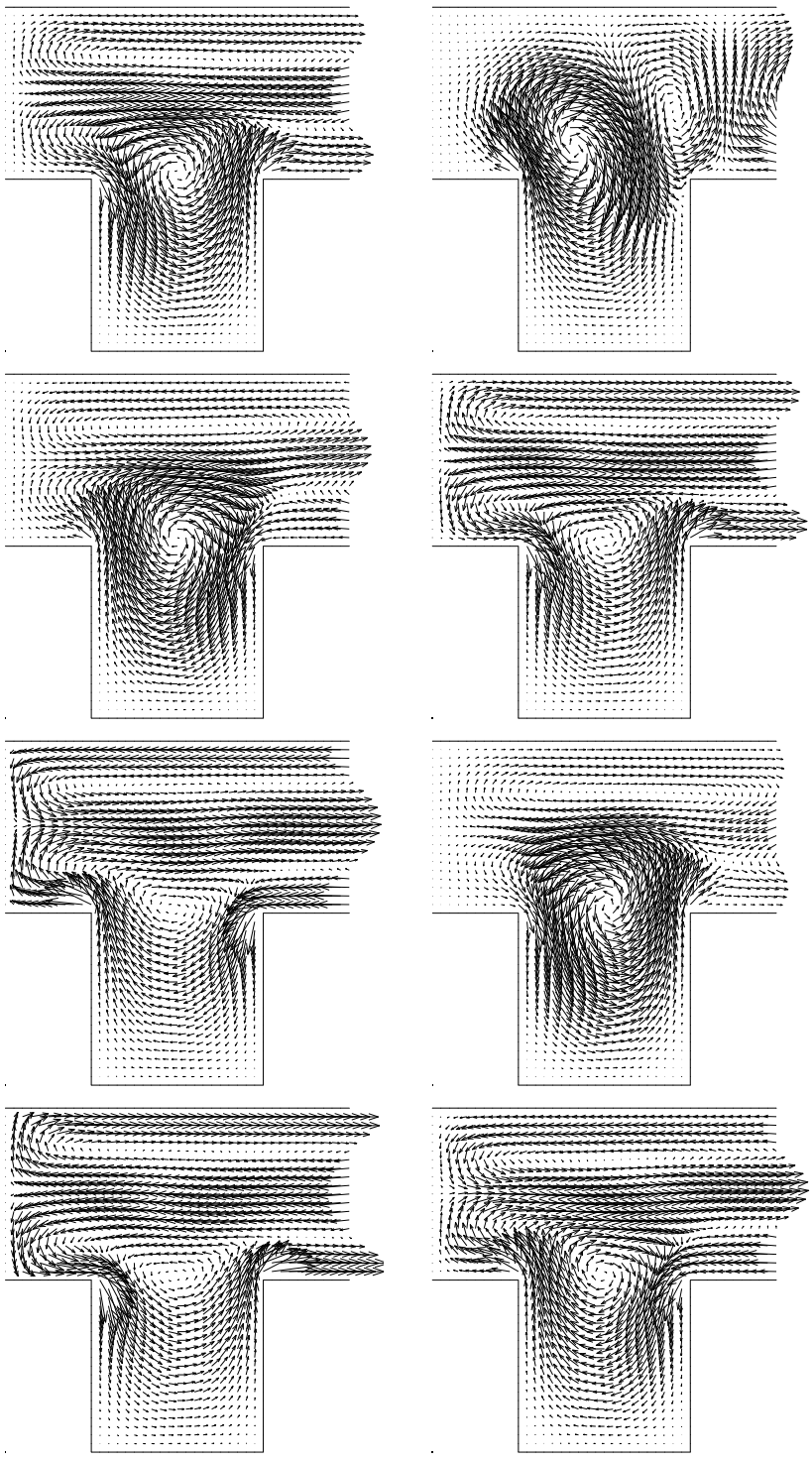

FIGURE 2. The CVT basis of cardinality 8 for the T-cell problem.

3.3. Determining CVT reduced-order approximations. We now use the Galerkin procedure discussed in Section 2.3 to determine a reduced-order approximation of the velocity field. The approximate velocity field $\mathbf{u}_{cvt}(\mathbf{x},t)$ is represented as a linear combination of the CVT basis functions as follows:

$$\mathbf{u}_{cvt}(\mathbf{x},t) = \alpha_0(t)\mathbf{v}(\mathbf{x}) + \sum_{k=1}^{K} \alpha_k(t)\mathbf{z}_k(\mathbf{x}), \tag{3.6}$$

where $\mathbf{z}_k$, $k = 1,\ldots,K$, denotes the k-th CVT basis function, $\alpha_k(t)$, $k = 1,\ldots,K$, the corresponding coefficient, $\mathbf{v}$ the reference solution used in Section 3.1 to modify the snapshots so that they satisfy homogeneous boundary conditions, $\alpha_0(t) = \gamma(t)/3$, and K the cardinality of the CVT basis set. In our computations, $K = 4$, 5, 6, 7, 8, 10, 12, or 16. The first term in (3.6) is included so that $\mathbf{u}$ satisfies the boundary condition (3.2).

Applying the Galerkin principle which forces the residual to be orthogonal to each of the basis functions, we obtain

$$\begin{aligned} \int_\Omega \frac{\partial}{\partial t}\mathbf{u}_{cvt}\cdot\mathbf{z}_i\,d\Omega + \nu\int_\Omega \nabla\mathbf{u}_{cvt} : \nabla\mathbf{z}_i\,d\Omega \\ + \int_\Omega (\mathbf{u}_{cvt}\cdot\nabla)\mathbf{u}_{cvt}\cdot\mathbf{z}_i\,d\Omega = 0 \qquad \text{for } i = 1,\ldots,K. \end{aligned} \tag{3.7}$$

Note that due to the fact that the basis functions $\mathbf{z}_k$, $k = 1,\ldots,K$, are discretely solenoidal, the pressure does not appear in this system. Using (3.6), it is easy to see that (3.7) is equivalent to the system of K nonlinear ordinary differential equations

$$\begin{aligned} &\sum_{k=1}^{K}\frac{d}{dt}\alpha_k(t)\Big(\mathbf{z}_k,\mathbf{z}_i\Big) + \nu\sum_{k=1}^{K}\alpha_k(t)\Big(\nabla\mathbf{z}_k,\nabla\mathbf{z}_i\Big) \\ &\qquad + \left(\sum_{\ell=1}^{K}\alpha_\ell(t)\mathbf{z}_\ell\cdot\nabla\sum_{k=1}^{K}\alpha_k(t)\mathbf{z}_k,\mathbf{z}_i\right) \\ &\qquad + \alpha_0(t)\sum_{k=1}^{K}\alpha_k(t)\Big(\mathbf{z}_k\cdot\nabla\mathbf{v} + \mathbf{v}\cdot\nabla\mathbf{z}_k,\mathbf{z}_i\Big) \\ &\quad = -\frac{d}{dt}\alpha_0(t)\Big(\mathbf{v},\mathbf{z}_i\Big) - \alpha_0(t)\Big(\alpha_0(t)-1\Big)\Big(\mathbf{v}\cdot\nabla\mathbf{v},\mathbf{z}_i\Big) \end{aligned} \tag{3.8}$$

along with the initial conditions

$$\sum_{k=1}^{K}\alpha_k(0)\big(\mathbf{z}_k,\mathbf{z}_i\big) = \big(\mathbf{u}_0 - \alpha_0(0)\mathbf{v},\mathbf{z}_i\big) \tag{3.9}$$

for $i = 1,\ldots,K$, where $(\cdot,\cdot)$ denotes the $L^2(\Omega)$ inner product. The set of ordinary differential equations (3.8)–(3.9) is solved by using a 4-th order Adam-Multon method.

3.4. Computational experiments. To illustrate the use and effectiveness of the low-dimensional, CVT-based reduced-order model, we choose two shapes for the inlet velocity factor $\gamma(t)$ and several different choices for the cardinality of the CVT basis set. The two choices for the inlet velocity factor $\gamma(t)$ are given by

- **Case 1:** a hat function with respect to time (see Figure 3)

$$\gamma(t) = \begin{cases} \frac{400}{3}t + 1 & \text{for } 0 \le t \le 0.03 \\ -\frac{400}{3}t + 9 & \text{for } 0.03 \le t \le 0.06 \end{cases}$$

- **Case 2:** a "general" function with respect to time (see Figure 3).

$$\gamma(t) = 3 + 2\cos(18\pi t)\sin(70\pi(t+10)) \quad \text{for } 0 \le t \le 0.06.$$

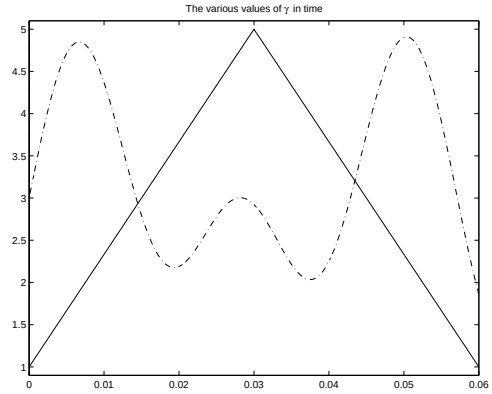

FIGURE 3. The two choices for the inflow function $\gamma(t)$; Case 1: solid curve; Case 2: dashed curve.

For both Case 1 and 2, solutions of the system (2.1), (2.2), and (3.1)–(3.4) were also approximated using the full finite element discretization employing thousands of unknowns.

Computing the CVT-based reduced-order solution for basis function sets of cardinality $K = 4$, 5, 6, 7, 8, 10, 12, and 16 allowed for a study of the behavior of the error in the reduced-order approximations. The L^2 error was computed at each time step, based on the difference between the full finite element and reduced-order solutions. The plots of these L^2 errors versus time are displayed in Figures 4 and 5 for Cases 1 and 2, respectively. We see that the CVT-reduced order model produces approximations that are quite accurate and generally improve as the cardinality of the basis increases.

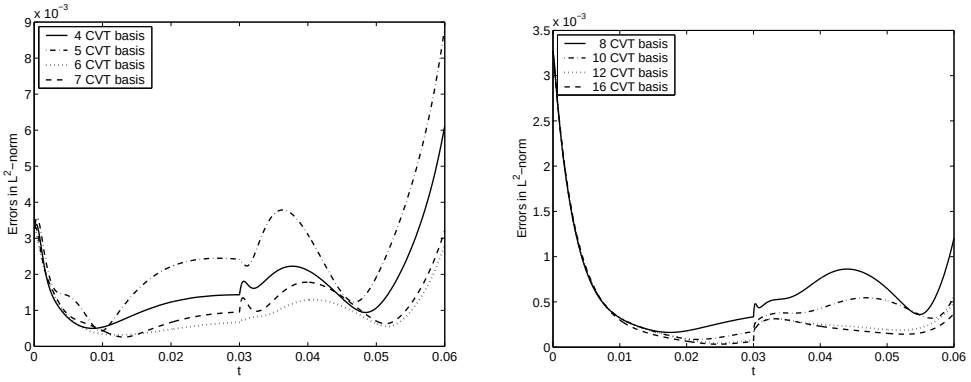

FIGURE 4. L^2-norm of difference between CVT-based reduced-order solutions and the full finite element simulation vs. time for Case 1.

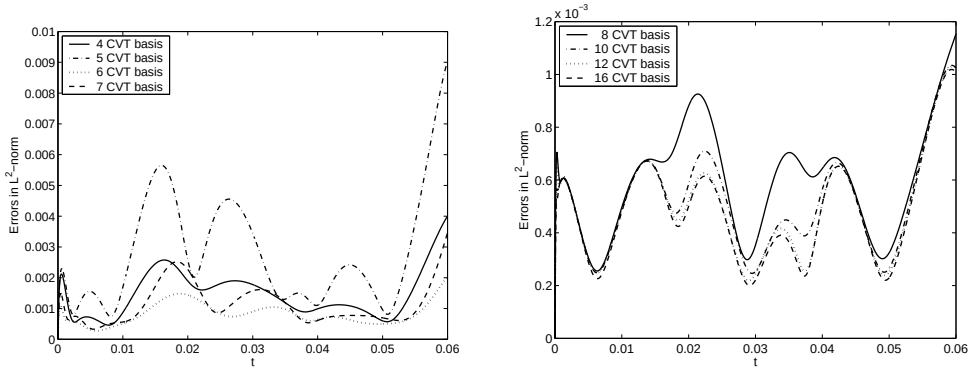

FIGURE 5. L^2-norm of difference between CVT-based reduced-order solutions and the full finite element simulation vs. time for Case 2.

It is of interest to compare the the CPU times for effecting a simulation of the T-cell problem using the CVT-based reduced-order model with that needed for a full finite element simulation. Such a comparison is given in Table 1 for the input data of Case 2 for computations carried out on a Dell Precision Workstation 650 with dual 3.02 Ghz CPU's. (It required 32855 sec to obtain 500 snapshots which recall were generated by a calculation over the shorter time interval $(0, 0.05)$.) We see from the table the tremendous reduction in computing time that is effected by using a reduced-order model.

Number of CVT basis functions	CPU time in seconds
4	0.641
5	0.719
6	1.375
7	2.078
8	3.515
10	8.093
12	15.438
16	52.438
Full FEM	39426.62

TABLE 1. CPU times for the Case 2 simulation for the CVT and full finite element models.

References

1. N. Aubry, W. Lian, and E. Titi, *Preserving symmetries in the proper orthogonal decomposition*, SIAM J. Sci. Comp. **14** (1993), 483–505.
2. G. Berkooz, P. Holmes, and J. Lumley, *The proper orthogonal decomposition in the analysis of turbulent flows*, Ann. Rev. Fluid. Mech. **25** (1993), 539–575.
3. G. Berkooz and E. Titi, *Galerkin projections and the proper orthogonal decomposition for equivariant equations*, Phys. Let. A **174** (1993), 94–102.

4. E. Christensen, M. Brons, and J. Sorensen, *Evaluation of proper orthogonal decomposition-based decomposition techniques applied to parameter-dependent nonturbulent flows*, SIAM J. Sci. Comp. **21** (2000), 1419–1434.
5. A. Deane, I. Kevrekidis, G. Karniadakis, and S. Orszag, *Low-dimensional models for complex geometry flows: applications to grooved channels and circular cylinders*, Phys. Fluids A **3** (1991), 2337–2354.
6. M. Graham and I. Kevrekidis, *Pattern analysis and model reduction: Some alternative approaches to the karhunen-lóeve decomposition*, Comp. Chem. Engng. **20** (1996), 495–506.
7. P. Holmes, J. Lumley, and G. Berkooz, *Turbulence, coherent structures, dynamical systems and symmetry*, Cambridge University Press, Cambridge, 1996.
8. P. Holmes, J. Lumley, G. Berkooz, J. Mattingly, and R. Wittenberg, *Low-dimensional models of coherent structures in turbulence*, Phys. Rep. **287** (1997), 337–384.
9. L. Ju, Q. Du, and M. Gunzburger, *Probablistic methods for centroidal Voronoi tessellations and their parallel implementations*, J. Parallel Comput. **28** (2002), 1477–1500.
10. K. Kunisch and S. Volkwein, *Control of Burger's equation by a reduced order approach using proper orthogonal decomposition*, JOTA **102** (1999), 345–371.
11. ———, *Galerkin proper orthogonal decomposition methods for parabolic problems*, Projektbereich Kontinuierliche Optimierung und Kontrolle, Spezialforschungsbereich F003 Optimierung und Kontrolle, Bericht Nr. 153, Graz, 1999.
12. J. Lumley, *Stochastic tools in turbulence*, Academic, New York, 1971.
13. H. Park and D. Cho, *Low dimensional modeling of flow reactors*, Int. J. Heat Mass Transf. **39** (1996), 3311–3323.
14. H. M. Park and J. S. Chung, *A sequential method of solving inverse natural convection problems*, Inverse Problems **18** (2002), no. 3, 529–546.
15. H. M. Park and Y. D. Jang, *Control of Burgers equation by means of mode reduction*, Internat. J. Engrg. Sci. **38** (2000), no. 7, 785–805.
16. H. M. Park and J. H. Lee, *Solution of an inverse heat transfer problem by means of empirical reduction of modes*, Z. Angew. Math. Phys. **51** (2000), no. 1, 17–38.
17. H. M. Park and M. W. Lee, *An efficient method of solving the Navier-Stokes equations for flow control*, Internat. J. Numer. Methods Engrg. **41** (1998), no. 6, 1133–1151.
18. H. M. Park and W. J. Lee, *A new numerical method for the boundary optimal control problems of the heat conduction equation*, Internat. J. Numer. Methods Engrg. **53** (2002), no. 7, 1593–1613.
19. M. Rathinam and L. Petzold, *Dynamic iteration using reduced order models: A method for simulation of large scale modular systems*, SIAM J. Numer. Anal. **40** (2002), 1446–1474.
20. ———, *A new look at proper orthogonal decomposition*, SIAM J. Numer. Anal. **41** (2003), 1893–1925.
21. S. Ravindran, *Proper orthogonal decomposition in optimal control of fluids*, Int. J. Numer. Meth. Fluids **34** (2000), 425–448.
22. ———, *Reduced-order adaptive controllers for fluid flows using POD*, J. Sci. Comput. **15** (2000), 457–478.
23. J. Rodríguez and L. Sirovich, *Low-dimensional dynamics for the complex Ginzburg-Landau equations*, Physica D **43** (1990), 77–86.
24. L. Sirovich, *Turbulence and the dynamics of coherent structures, I-III*, Quart. Appl. Math. **45** (1987), 561–590.
25. N. Smaoui and D. Armbruster, *Symmetry and the Karhunen-Loève analysis*, SIAM J. Sci. Comput. **18** (1997), 1526–1532.
26. S. Volkwein, *Proper orthogonal decompositionand singular value decomposition*, Projektbereich Kontinuierliche Optimierung und Kontrolle, Spezialforschungsbereich F003 Optimierung und Kontrolle, Bericht, Nr. 153, Graz, 1999.
27. ———, *Optimal control of a phase field model using the proper orthogonal decomposition*, ZAMM **81** (2001), 83–97.

School of Computational Science, Florida State University, Tallahassee FL 32306-4120

Department of Mathematics, Ajou University, Suwon 442-749, Korea
E-mail address: hclee@mac.com